CHEMISTRY OF MATERIALS

Article

pubs.acs.org/cm

Influence of Surface Termination on the Energy Level Alignment at the $CH_3NH_3PbI_3$ Perovskite/C60 Interface

Claudio Quarti,*[,†] Filippo De Angelis,[‡,§] and David Beljonne[†]

[†]Laboratory for Chemistry of Novel Materials, Department of Chemistry, Université de Mons Place du Parc 20, 7000 Mons, Belgium
[‡]Computational Laboratory for Hybrid/Organic Photovoltaics (CLHYO), CNR-ISTM, I-06123 Perugia, Italy
[§]CompuNet, Istituto Italiano di Tecnologia, Via Morego 30, 16163 Genova, Italy

Supporting Information

ABSTRACT: The impressive photovoltaic performance of hybrid iodide $CH_3NH_3PbI_3$ perovskite relies, among other factors, on the optimal alignment of the electronic energy levels of the semiconductor with respect to conventional hole transporting (HTM) and electron transporting (ETM) materials. Here, we first report on density functional theory electronic structure calculations of slab models of the (001) surface aiming to assess how the perovskite valence and conduction band edge (VBE and CBE) energies depend on the nature of the surface exposed to vacuum. We find that the surface termination plays a critical role in determining the energies of the frontier crystal orbitals, with PbI-terminated surface showing VBE and CBE energy ∼1 eV below the corresponding levels in the methylammonium-terminated surfaces. We next build perovskite/C60 interfaces based on two such surfaces and discuss the associated electronic structure in light of recent experimental data. The two interfaces are rather inert showing limited band bending/shifts with respect to the isolated components, in line with photoelectron spectroscopy data. They, however, yield very different electron extraction energies, possibly explaining the different behaviors reported in the literature.

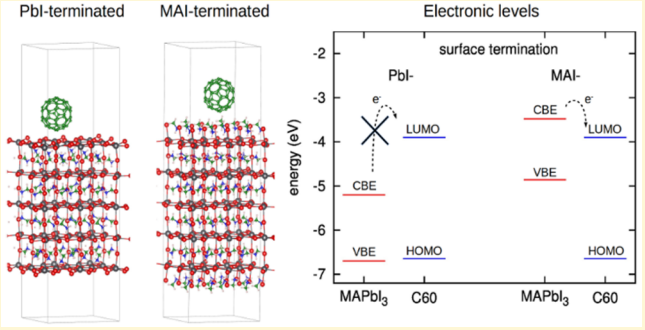

INTRODUCTION

Hybrid organometal perovskites are rapidly emerging as serious contenders to rival the leading photovoltaic (PV) technologies. In just a few years, perovskite-based devices have demonstrated a drastic improvement in photon-to-current conversion, with solar cell quantum efficiencies currently reaching ∼20%.[1−6] The key factors at the origin of the impressive photovoltaic performances of this class of materials are undoubtedly associated with their inherent chemical−physical properties, as a tunable band gap,[7] ambipolar charge transport properties[8−10] with high charge carrier mobilities (∼27 $cm^2\ V^{-1}\ s^{-1}$),[11−13] large optical absorption coefficient (∼$10^5\ cm^{-1}$),[14] and reduced bimolecular charge recombination.[15] On the other hand, for the effective functioning of solar cells, surface and interface properties are of paramount importance. In particular, the energetic position of the valence and conduction band edges plays an important role, as they dictate the efficiency of the charge extraction at the respective electrodes. Several recent publications employed UV-photoemission spectroscopy (UPS) or inverted photoemission spectroscopy (IPES) to investigate the energy level alignment of the frontier electronic levels between hybrid perovskites and many popular hole transporting materials (HTMs), electron transporting materials (ETMs), and substrates.[16−22] These works mainly focused on $CH_3NH_3PbI_3$ (here-on $MAPbI_3$), and they highlighted a positive matching between the energy level positions of the valence band edge, (VBE ∼ 5.4 eV) and conduction band edge (VBE ∼ 3.7 eV) of this material with respect to a large variety of electron and hole transporting materials of interest, such as TiO_2,[16] C60,[17,21] carbon nanotubes,[18] and several substrates.[22]

Theoretical investigations have contributed to a basic understanding of perovskite surfaces and interfaces. Haruyama et al. investigated the thermodynamic stability of several surface models that differ by the surface termination. Considering surface models exposing lead and iodide atoms, they computed the energy associated with the introduction of vacant defects, finding a larger stability for vacant models. Moreover, these authors found that none of the surfaces investigated have midgap states, which would be detrimental for the photovoltaic working mechanism.[23] Apart from the inherent stability of the specific surface terminations of the hybrid perovskites, this class of materials is also very sensitive to degradation induced by the atmosphere.[24] The first investigations pointed out toward a negative role of moisture on the stability of perovskite, and, in two independent studies, Mosconi et al.[25] and Koocher et al.[26] provided a detailed theoretical investigation on the mechanisms of degradation induced by water at the $MAPbI_3$ surface. In particular, Mosconi et al. found a different resistance of the

Received: August 5, 2016
Revised: January 16, 2017
Published: January 17, 2017

DOI: 10.1021/acs.chemmater.6b03259
Chem. Mater. 2017, 29, 958−968

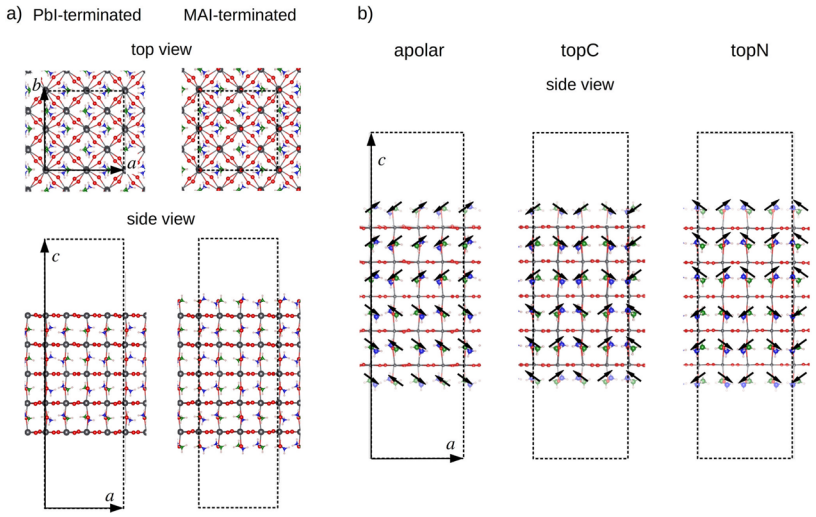

Figure 1. Slab models employed for the simulation of the $MAPbI_3$ (001) surface: (a) PbI- and MAI-terminated surfaces; (b) orientation of the MA cations (apolar, topC, topN) with respect to the (001) surface. The arrows represent the orientation of the MA cations, with the arrowhead in correspondence with the NH_3 group, consistently with the molecular dipole.[37] The color map is lead = black, iodide = red, carbon = green, nitrogen = blue, and hydrogen = white.

perovskite surface with respect to two possible surface terminations: A PbI-terminated surface, exposing lead and iodide atoms, as in the work of Haruyama, and a MAI-terminated surface, exposing methylammonium cations (MA) and iodide atoms. More specifically, Car–Parrinello molecular dynamics simulations indicate that the PbI-terminated surface is more resistant to water degradation, while the MAI-terminated surface is easily degraded, with removal of the upper atoms resulting in the formation of a PbI-terminated surface.[25] Recent findings are pointing out also an inherent sensitivity of hybrid perovskite toward oxygen.[27] On the other hand, a comprehensive understanding of the electronic properties of the $MAPbI_3$ surface is still lacking, to the best of our knowledge. To explain the temperature dependence of the valence band position of the $MAPbI_3$ perovskite, Foley et al. computed the energy position of the valence band edge of $MAPbI_3$, at ∼5.7 eV, in reasonably good agreement with experiment (5.4 eV).[28] Yin et al. provided a joined experimental/theoretical study on the energy level alignment of the $MAPbI_3$ perovskite with one typical HTM and one ETM, spiro-OMeTAD and C60, respectively.[19] However, none of these works provide a detailed picture on how the electronic structure of the $MAPbI_3$ perovskite is affected by the surface structural parameters, including the orientation of the MA cations and the surface termination.

Here, by means of density functional theory (DFT) simulations of slab models of $MAPbI_3$, we show that the surface termination has a tremendous impact on the energy of the VBE and CBE states. PbI-terminated surfaces yield VBE and CBE ∼1 eV lower in energy with respect to MAI-terminated surfaces, with the latter likely corresponding to the surfaces investigated in the literature using photoelectron spectroscopy,[16−20,22] as also confirmed by recent STM investigations.[29,30] We also study the interface between $MAPbI_3$ and C60, a highly relevant interface as the corresponding solar cells feature excellent quantum yields (∼14%)[31] and reduced current–voltage hysteresis issues.[32] From our DFT simulations, we find that the 0.3 eV upshift of the C60 levels measured by Schulz et al. at the $MAPbI_3$/C60 interface[17] can be explained on the basis of an electron transfer from the perovskite to the C60. Most importantly, we also infer from these calculations that the 1 eV discrepancy between the VBE and CBE energies reported by several authors[16−20,22] and by Lo et al.[21] is likely the result of probing different surface terminations. Our results suggest that a fine control on the surface topology of $MAPbI_3$ is essential to obtain the proper energy level alignment in perovskite-based solar cell devices.

■ COMPUTATIONAL METHODS AND MODELS

In Figure 1, we portray the slab models employed in the present work. Considering the tetragonal phase of $MAPbI_3$, which is stable at room temperature,[33] (001) and (110) are the only flat, neutral surfaces. These are thus expected to be the most stable perovskite surfaces, as supported by DFT calculations performed by Haruyama et al.[23] and Yin et al.[19] In this work, we consider slab models of the (001) surface but we verify for one selected case that the surface (110) provides similar results. Our slab models have a 2 × 2 periodicity in-plane (see Figure 1a) and are five PbI_2 layers thick (see Figure 1b).

As discussed in the Introduction, Mosconi et al. pointed out a resistance of the $MAPbI_3$ surface to water degradation that is sensitive to the surface termination, with the PbI-terminated surface being more resistant than the MAI-terminated one.[25] For this reason, we here consider these two surface topologies (see Figure 1a). We also envision different orientations of the MA cations, as it has important indirect effects on the properties of the $MAPbI_3$ perovskite.[34−36] As a matter of fact, domains with a global alignment of MA cations result in a ferroelectric character of the perovskite,[34,37−39] which implies a spatial band bending of the electronic levels and their localization in specific material regions,[34] together with other exotic phenomena such as the Rashba–Dresselhaus effect.[34,40,41] Yet, the possibility to find large domains in $MAPbI_3$ with a global alignment of the MA cations has been largely criticized recently,[34,42] in view of the fast reorientational motion of the MA cations at room temperature.[33,43,44]

To take into account these orientational effects, we built three different models (see Figure 1b): (i) in the *apolar* model, the MA cations in each layer have an isotropic orientation with respect to the slab thickness; i.e., half of the MA cations have their -NH_3 groups pointing up (and half pointing down). (ii) In the *topC* model, the MA cations have their -CH_3 groups oriented toward vacuum in all layers. (iii) In the *topN* model, the MA cations are instead oriented with their -NH_3 groups pointing to vacuum. Notice that all of the slab models are neutral and symmetric with respect to the central Pb–I plane (see Figure 1b), as widely suggested in the literature, to avoid the

DOI: 10.1021/acs.chemmater.6b03259
Chem. Mater. 2017, 29, 958−968

aforementioned effects associated with the formation of a polar slab.[45−47] We employed the lattice parameters from Poglitsch and Weber for the tetragonal phase of $MAPbI_3$ at room temperature ($a = b = 8.8556$ Å),[33] and we used 60 Å along the slab thickness, which results in 30 and 20 Å of vacuum between a slab and its periodic replica respectively for the PbI- and MAI-terminated models.

We performed DFT periodic calculations using the PWscf package of the Quantum Espresso suite program.[48] Since van der Waals interactions play a major role on the stability of the perovskite C60 interface, we resorted to the vdw-DF2 functional for the exchange correlation.[49] We employed ultrasoft,[50] scalar-relativistic pseudopotentials, together with a cutoff of 25 and 200 Ry, for the expansion of the wave function and density, respectively. For the sampling of the first Brillouin zone, we considered only the Γ point. This computational setup revealed it was effective in several recent studies.[34,51] Bader charge analysis was performed using the program from ref 52. For the perovskite/C60 interface, we used the dipole correction for the electrostatic potential, to take into account unavoidable asymmetry in the electrostatic potential.[53]

RESULTS AND DISCUSSION

$MAPbI_3$ Surface. We fully relaxed the atomic positions of the six structural models under investigation. In general, the MA cations did not change their orientation during the optimization, except for the case of the MAI-terminated, topN model, where all the MA cations of the outermost layers rotate toward the underlying PbI_2 layer. A similar result was found by Mosconi et al. using Car−Parrinello molecular dynamics simulations.[25] These authors associated this peculiar reorientation of the MA cations to weak intermolecular interactions, which were taken into account using the Grimme correction scheme.[54] Here, we thus confirm this interpretation and further notice that such a reorientation of the outlying MA cations predicted when using the vdw-DF2 functional is not observed if instead the PBE functional is adopted (see the Supporting Information), hence pointing to the importance of properly including van der Waals interactions for the description of the orientation of the MA cations at the surface.

We first discuss the energetics of the slab models studied. As the focus of the present work is on the electronic properties of $MAPbI_3$ at the surface, we do not present a detailed study of complex structural phenomena such as surface reconstruction, which besides have been ruled out by recent STM measurements.[29,30] In Table 1, we report the relative energies of the perovskite MAI- and PbI-terminated models. For the MAI-terminated surfaces, the most stable structure is the topC, while the topN and apolar structures lie respectively ∼1 and ∼3 k_BT/$MAPbI_3$ higher in energy. For the PbI-terminated surfaces, the topN model is found to be the most stable, while the other models lie slightly higher in energy, within ∼1k_BT per $MAPbI_3$ unit at room temperature. Dealing with the relative stability of the two terminations, we cannot directly compare the energetics of MAI- and PbI-terminated models, as they have different stoichiometries ($MA_{48}Pb_{40}I_{128}$ and $MA_{32}Pb_{40}I_{112}$, respectively). To take this difference into account, we have normalized their energetics with respect to the same amount of atoms, subtracting/adding the contributions from the 8 MA···I units in excess/missing in the MAI-/PbI-terminated models, respectively, to reach the regular perovskite stoichiometry. We report the detailed procedure in the Supporting Information. We found that, whatever the orientation of the MA cations considered, the MAI-terminated surface is significantly more stable than the PbI-terminated one, with an energy difference on the order of 830−860 meV per $MAPbI_3$ units ($\gg k_BT$ at room temperature). This suggests that the MAI termination should be the preferred thermodynamic surface under ideal conditions, in agreement with recent STM measurements.[29,30]

Table 1. Stability and Electronic Band Gap of the $MAPbI_3$ Slab Models Investigated

orientation	stability		band gap	
	MAI	PbI	MAI	PbI
	(meV/$MAPbI_3$ unit)		(eV)	
apolar	80.3	849.5	1.82	1.15
topC	0.0	857.9	1.85	1.17
topN	24.0	829.2	1.45	1.36
expt			1.55[a] - 1.70[b]	

[a]Reference 55. [b]Reference 16.

We now discuss the electronic properties of the studied $MAPbI_3$ slab models. The electronic band gaps computed at the DFT level for the various slab models are listed in Table 1. Namely, while the DFT band gaps for the PbI-terminated slabs are smaller than the corresponding experimental data measured in the bulk by UV−vis spectroscopy (∼1.55 eV)[55] or on the surface by UPS/IPES (1.7 eV),[16] the corresponding values for the MAI-terminated surfaces are generally slightly larger than experiment. In line with earlier work by Haruyama et al., we find no evidence for the formation of midgap surface states.[23] It is worth mentioning that the computational approach employed here, namely, scalar-relativistic DFT calculations at the GGA level, correctly predicts the band gap for the bulk $MAPbI_3$ perovskite,[56] because of a fortuitous cancellation of errors between relativistic, spin−orbit coupling and electronic correlation, as widely reported in the literature.[57,58] For a robust description of the electronic properties of this material, we should resort to more involved computational approaches, as hybrid DFT[59] or GW approximation[40,60] with inclusion of the spin−orbit coupling, but these approaches are not feasible in the present case, because of the size of the models studied.

We now pass to the evaluation of the VBE and CBE energies and of the work function (Φ), which are easily accessible from slab calculations.[61−63] Figure 2a displays the energy of the VBE and CBE of the six slab models investigated (solid line), together with the work function (dashed line). Very strikingly, we find that the work function, and correspondingly the VBE and CBE, is highly sensitive to the surface termination. The calculated work function is between 1 and 1.5 eV lower for the PbI-terminated structures compared to the MAI-terminated structures. Also the orientation of the MA cation plays a role in the magnitude of the work function, which increases going from the topN to the apolar, to the topC orientation. Yet this effect is smaller with respect to that of the surface termination. As shown in Figure 2a, the agreement between calculated VBE and CBE energies with respect to the experimental data is rather limited, though a slightly better agreement is found for the MAI-terminated structures. This is most likely due to the aforementioned limitations of the computational approach used. In fact, even if the band gap of $MAPbI_3$ predicted at the GGA level is in reasonable agreement with the experiment, no definitive conclusions can be drawn from this on the accuracy of the computed VBE and CBE energies. In this sense, a previous study on metallic systems suggests that GGA

DOI: 10.1021/acs.chemmater.6b03259
Chem. Mater. 2017, 29, 958−968

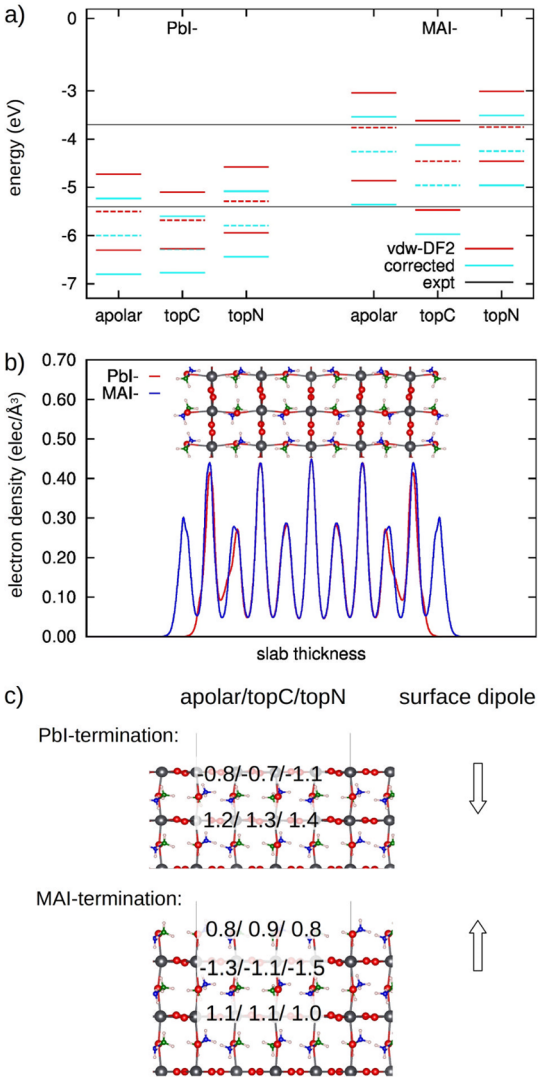

Figure 2. (a) VBE and CBE energies (solid lines) and work function (dashed line) of the $MAPbI_3$ slab models, at the vdw-DF2 level and corrected as described in the main text (see main text), in comparison with the experimental VBE and CBE from ref 17 (black solid line). (b) Electronic density on the PbI- and MAI-terminated model averaged along planes orthogonal to the slab normal direction (the apolar slab model is reported as reference). (c) Average nominal charge for outmost layers for the apolar/topC/topN orientation and resulting surface dipole (the charge was obtained averaging the Bader charge of the atoms lying on a given layer and subtracting the nominal charge).

calculations are less accurate for the description of surface properties as compared to bulk properties.[64] The use of more involved computational approaches is not feasible in the present case, but we can still correct for the effect of spin−orbit coupling and electronic correlation on the VBE and CBE energy as follows. In a recent work, Menéndez-Proupin et al.[59] computed the energies of the VBE and CBE of the $MAPbI_3$, referred to the averaged electrostatic potential in the unit cell, comparing the results without/with spin−orbit coupling and using a less/more accurate treatment of the electronic correlation (respectively GGA and hybrid functionals).[59] They found that the inclusion of spin−orbit coupling and the accurate treatment of the electronic correlation results in a downshift by 0.40 and 0.47 eV of the VBE and CBE, respectively (with respect to a reference corresponding to the averaged electrostatic potential in the cell). The asymmetry in the VBE and CBE correction is also consistent with the results from SOC-GW calculations, which show a 1.08 eV band gap decrease associated with SOC, which slightly surpasses the 1.0 eV band gap increase due to the electronic correlation.[60] Applying these shifts for the computed VBE and CBE, we obtain the "corrected" level alignment reported in Figure 2a, which brings the energy levels of the MAI surface in good agreement with the experimental data. Before proceeding, we highlight that the changes in the energy position of the frontier crystal orbitals discussed here occur with respect to the vacuum level, which is taken as a reference (zero energy) in all our work.

The 1−1.5 eV difference between the work functions of the PbI and MAI surfaces, and consequently of the VBE and CBE, stems from the different electronic density distributions at the surface. The planar averaged electronic density in Figure 2b points out that the PbI- and MAI-terminated surfaces expose to the surface an electron enriched and an electron tapered layer, respectively. The Bader analysis performed on the outmost layers of our slab models confirms that an electron transfer takes place from the MAI to the PbI layers, as shown in Figure 2c, with the consequent formation of a surface dipole, pointing in opposite directions for the two terminations. This surface dipole is responsible for the upshift and the downshift of the vacuum level, respectively for the MAI and for the PbI termination, as indicated by the Helmholz equation:

$$\Delta\mathrm{vac} = -\frac{\mu}{\varepsilon_0 A}$$

(where μ is the component of the surface dipole normal to the surface, ε_0 is the dielectric constant in vacuum, A is the surface area, and Δvac is the shift of the vacuum level).[61,65] This mechanism is depicted in Figure 3a. Also the role of the MA cation orientation can be rationalized as an independent contribution to the surface dipole due to the polarization of the

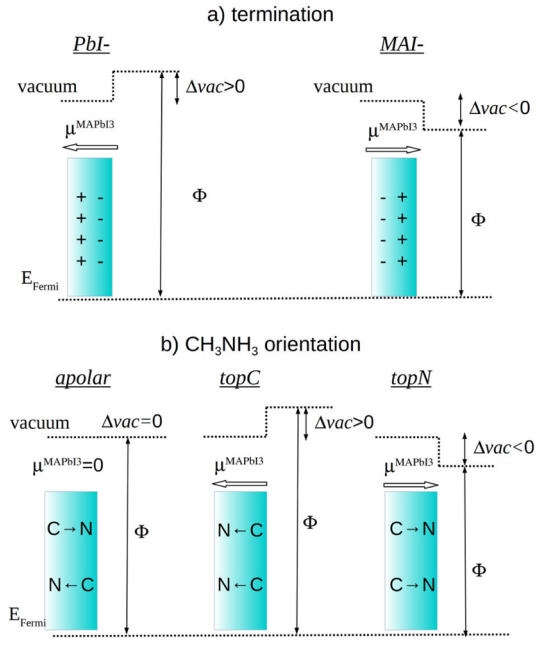

Figure 3. Shift of the vacuum level on $MAPbI_3$ slab model due to the surface dipole associated (a) with the surface termination and (b) to the MA cation orientation.

DOI: 10.1021/acs.chemmater.6b03259
Chem. Mater. 2017, 29, 958−968

outmost layer. In $MAPbI_3$ with oriented MA domains, the polarization follows the orientation of the MA cations, going from the CH_3 group to the NH_3 group.[37] This results in null, positive, and negative dipolar contributions to the surface dipole respectively in the case of the apolar, topC, and topN orientations, which in turn correspond to null, positive, and negative contributions to the shift of the vacuum level, as sketched in Figure 3b.

The fact that the MAI-terminated surface likely corresponds to the one probed in the various UPS studies reported in the literature[16−20,22] is in line with several results: (i) the MAI termination is significantly more stable than the PbI termination, in vacuum (see Table 1); (ii) the band gap of the MAI-terminated models (1.85−1.45 eV) is in closer agreement to the band gap measured experimentally (1.55−1.7 eV) than the band gap of the PbI models (1.15−1.36 eV); (iii) the energies of the VBE and CBE of the MAI terminations are closer to the experimental data, after correcting for the presumed effects of spin−orbit coupling and electronic correlation effects. In addition, a strong support to this assignment comes from two recent studies, showing that the STM imaging of the $MAPbI_3$ surface is consistent with the MAI termination (with small reorganization) and excluding the PbI termination.[29,30] As a final comment, we argue that if the MAI-terminated surface is indeed the one probed in most UPS measurements,[16−20,22] it might still be possible to observe surfaces with VBE and CBE lying some ∼1 eV lower than the −5.4 and −3.7 eV data reported in the literature and that would correspond to PbI-terminated perovskites. We conjecture that this was observed by Lo et al.[21] We will come back to this case when discussing the electronic structure at $MAPbI_3$/C60 interfaces later.

Before proceeding, we demonstrate that the difference in the energetics of the frontier orbitals of PbI- and MAI-terminated surfaces is a general result. We could wonder, for instance, whether this difference is an artifact associated with the limited thickness of our models or is specific to our choice of the (001) surface (rather than the (110) one). Dealing with the slab thickness, we have performed additional calculations and compared the VBE and CBE energies of the slabs in Figure 2a with thinner slabs (three PbI_2 layers) and thicker slabs (seven PbI_2 layers). The latter calculation is very expensive (more than 2500 electrons), and we thus limited it only to the apolar orientation. We find that the thickness of the model affects the VBE and CBE position up to ∼0.2 eV but the ∼1 eV difference between MAI- and PbI-terminated energy levels is preserved (see the Supporting Information). This insensitivity of the energy of the electronic levels with respect to the layer thickness is easily explained by the Helmholz equation, since, for slabs of sufficient thickness, the electronic and structural features taking place locally at the surface and determining the surface dipole moment μ have converged with slab vertical size. Regarding the influence of the surface, we calculated the electronic structure for a slab model of the (110) surface of the $MAPbI_3$ tetragonal phase, using the topC model as test case, and we found that VBE and CBE energies are upshifted by at most 0.36 eV, but again the ∼1 eV difference in the energy level position of PbI- and MAI-terminated surfaces still holds (see the Supporting Information).

Perovskite/C60 Interfaces. We now move on to the case of $MAPbI_3$ covered with C60 monolayers. Following similar works in the literature,[19] we have introduced one C60 molecule in contact with the various perovskite slab models from above, considering several initial positions of the C60 on the $MAPbI_3$ surface, in relation to the chemistry of the perovskite surface; see Figure 4. We then performed a full structural relaxation of the various models, introducing a dipole correction along the slab normal direction and self-consistently accounting for van der Waals interactions by means of the vdw-DF2 exchange-correlation functional. The interaction energies for the formation of a C60 adlayer on the perovskite surfaces are summarized in Table 2. These range from 0.3 to 1.0 eV per C60 (to put things in perspective, these values are comparable with the energy of the hydrogen bonding in nylons).[66] PbI-terminated models show generally stronger interactions, with ∼0.8 eV interaction energy on average, with respect to MAI-

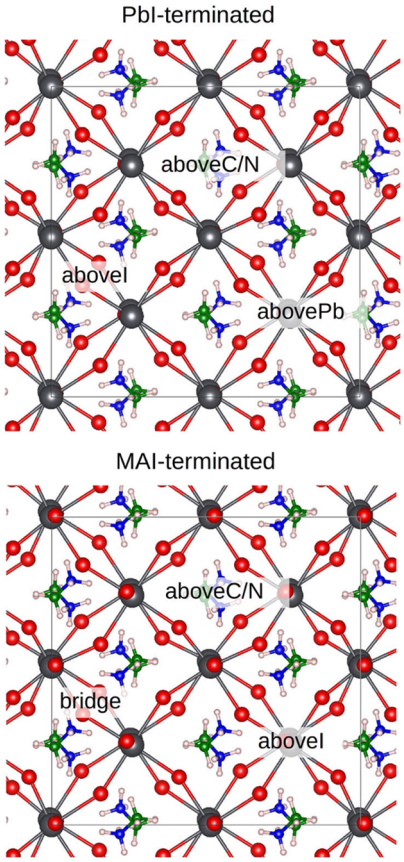

Figure 4. Position of the C60 with respect to the $MAPbI_3$ surface, for the PbI- (top panel) and the MAI-terminated (bottom panel) surfaces.

Table 2. Interaction Energy (eV per C60) of the Perovskite/C60 System, For the Various Investigated Models

C60	apolar	topC	topN
	PbI-Terminated		
aboveC	−0.69	−0.80	
aboveI	−0.97	−0.92	−0.75
aboveN	−0.52		−0.75
abovePb	−0.82	−0.80	−0.79
	PbI-Terminated		
aboveC	−0.53	−0.35	−0.31
aboveI	−0.51	−0.34	−0.40
aboveN	−0.36		
bridge	−0.66	−0.57	−0.56

DOI: 10.1021/acs.chemmater.6b03259
Chem. Mater. 2017, 29, 958−968

terminated ones, yielding average values of ∼0.4 eV. For both the PbI and MAI terminations, the stronger interactions take place when C60 is on top of the inorganic atoms (C60 in topI/topPb position for PbI-terminated and topI/bridge for MAI-terminated surfaces). This is fully expected, as iodine and lead are the most polarizable atoms, hence the larger van der Waals interactions.

We now treat in detail the electronic properties of the $MAPbI_3$/C60 interface, first discussing the energy level alignment for the noninteracting $MAPbI_3$ and C60 components and then considering the effects of interactions with the adlayer. In Figure 5a, we depict the energetics of the frontier electronic

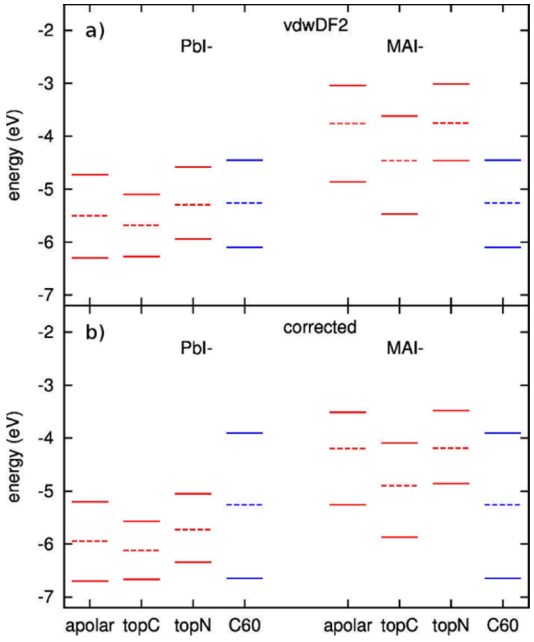

Figure 5. Energy level alignment (a) for the noninteracting $MAPbI_3$ (red) and C60 (blue) components, computed using vdw-DF2 functional, and (b) after introducing a correction *a posteriori* on the energy levels for the limitations of the computational method employed, as explained in the main text. Solid lines correspond to VBE/HOMO and CBE/LUMO levels, while dashed lines correspond to the work function (Φ).

levels of the perovskite slab models and of the C60, as obtained from two sets of independent DFT calculations. For the PbI termination, the LUMO level of the C60 lies above the CBE of the perovskite, which should prevent a spontaneous electron injection from the perovskite to the C60, while for the MAI termination the LUMO of the C60 lies below the CBE of the perovskite, allowing for the electron injection into the C60. Notice also that, for the MAI-terminated surface, the LUMO of the C60 is very close in energy to the VBE of the perovskite, a detrimental situation for the photovoltaic response as it would favor charge recombination at the interface. This unfavorable energy level alignment for the MAI termination is mainly due to inherent limitations of the computational approach employed, which describes the $MAPbI_3$ and C60 components with different accuracy. With regard to the perovskite, we already commented on the absence of spin−orbit coupling and the improper description of the electronic correlation and we proposed an *a posteriori* downshift correction of 0.40 and −0.47 eV for the VBE and CBE, respectively.[59,60] Similarly, it is well-known from the literature that the band gap of C60 is strongly underestimated by DFT. We have thus corrected the energy levels of C60 with respect to the inherent limitations of DFT, in line with the approach used for the $MAPbI_3$. For the C60 in the solid state, Shirley and Louie found that the DFT band gap (1.04 eV) is much improved when including correlation effects using the many-body perturbative GW method (2.15 eV to be compared with 2.5−2.6 eV found experimentally).[67] Unfortunately, these authors did not discuss whether this band gap opening, associated with the improved description of the electronic correlation by the GW method, is due to a 1.10 eV downshift of the HOMO, a 1.10 eV upshift of the LUMO, or any intermediate situation. Other simulations at the GW level performed by Qian et al. on an isolated C60 molecule, for which the absolute energy of the electronic levels is a well-defined quantity, shows that the 1.10 eV band gap opening is due to a symmetric 0.55 eV downshift and upshift of the occupied and unoccupied levels, respectively.[68] We thus propose an *a posteriori* correction of the energy levels of the C60 by −0.55 and +0.55 eV, respectively for the occupied and unoccupied levels, in parallel to the correction introduced for the energy levels of the perovskite. The "corrected" energy level alignment for the noninteracting $MAPbI_3$/C60 is reported in Figure 5b. Once these corrections are considered, the relative positions of the LUMO of C60 and CBE of $MAPbI_3$ are unvaried but the energy offset between the electronic levels of the noninteracting $MAPbI_3$ and C60 is in much better agreement with the available experimental data.[16,17,69] For the MAI surfaces, the LUMO of the C60 lies a few tenths of an electronvolt below the CBE of $MAPbI_3$, still allowing for the electron injection to C60, and more than 1 eV above the VBE of $MAPbI_3$, reducing the charge recombination at the interface. For the PbI surfaces, the LUMO of C60 is more than 1 eV higher in energy than the CBE of $MAPbI_3$, thus making the electron injection from the latter to the former strongly unfavorable.

We now discuss the energy alignment of the interacting $MAPbI_3$/C60 system. The effect of supramolecular interactions on the energy level alignment can be rationalized by the following three mechanisms: reciprocal polarization of $MAPbI_3$ and C60, charge transfer, and hybridization. (i) In the polarization mechanism, the partial positive/negative charge of the MAI-/PbI-terminated surface polarizes the C60, which in turns assumes a dipole in the direction of the surface dipole of the perovskite (see Figure 6a). As a result, the effect of the surface termination of $MAPbI_3$ on the vacuum level shift is enhanced by the C60, thus resulting in a further downshift/upshift of the vacuum level for the MAI-/PbI-terminated surface, respectively. (ii) In the charge transfer mechanism, the offset of the Fermi level of the C60 and of the perovskite promotes a partial electron transfer between the two components, inducing a surface dipole that in turn shifts the vacuum level. In light of the Fermi level alignment in Figure 5, the PbI surface allows for a charge transfer from the C60 to the perovskite, resulting in a downshift of the vacuum level, while the MAI surface is expected to yield a charge transfer in the opposite direction, namely, from the perovskite to C60, and a consequent upshift of the vacuum level; see Figure 6b. Notice that the vacuum level shifts induced by the polarization (Figure 6a) and by the charge transfer mechanisms (Figure 6b) for the MAI and the PbI surface are opposite, and thus easy to disentangle. (iii) In the hybridization mechanism, the electronic states of the perovskite and of the C60 mix, resulting in an unpredictable change in the vacuum level and, likely, in

DOI: 10.1021/acs.chemmater.6b03259
Chem. Mater. 2017, 29, 958−968

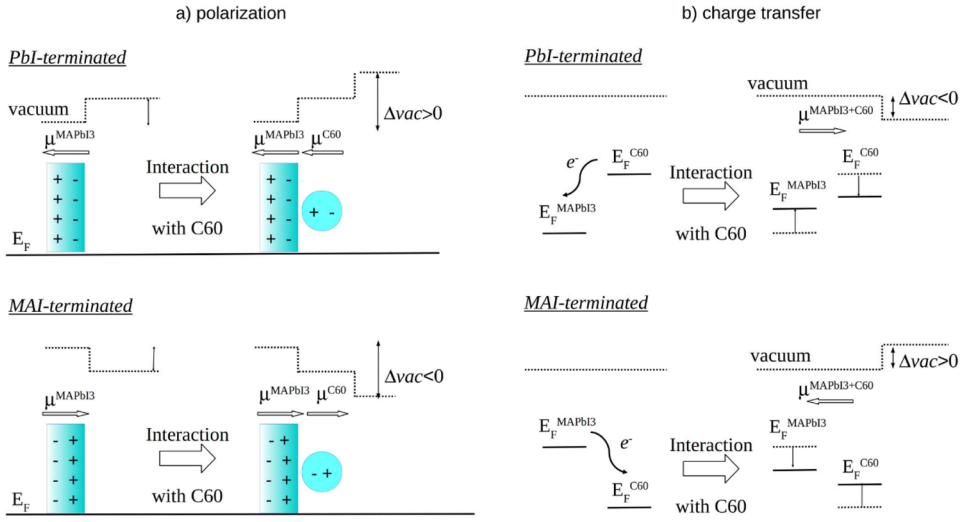

Figure 6. Variation of the vacuum (Δvac) and Fermi level (E_F) of the interacting $MAPbI_3$/C60 system induced by (a) reciprocal polarization of the $MAPbI_3$ and C60 and (b) by a charge transfer between $MAPbI_3$ and C60.

appreciable changes in the density of states of $MAPbI_3$ and C60.

In Figure 7a,b, we illustrate the previous concepts for two selected cases of the MAI and PbI termination, respectively. For the MAI surface, we considered the topN model with C60 in the bridge position; see Figure 7a. Going from the noninteracting to the interacting case, the DOS of the perovskite remains unvaried, while the levels of the C60 upshift by 0.05 eV, following the upshift of the vacuum level, and the HOMO slightly broadens. The 0.05 eV upshift of the vacuum level is not consistent with the polarization mechanism in Figure 6a, while it is consistent with the charge transfer mechanism in Figure 6b. The charge transfer mechanism is also in line with the alignment of the Fermi energies of the two noninteracting components and is confirmed by the Bader charge analysis, which highlights an electron transfer from $MAPbI_3$ to C60 of ∼0.02 electrons per C60. In the right panel of Figure 7a, we report the difference of the electronic density of the coupled $MAPbI_3$/C60 system and those of the isolated fragments, showing the electron reorganization following the intermolecular interactions. For the PbI termination instead, we considered the apolar model with the C60 in the aboveI position; see Figure 7b. The energy levels of the C60 downshift, following the 0.32 eV downshift of the vacuum level, which rules out again the polarization mechanism and supports the charge transfer from the C60 to $MAPbI_3$. This mechanism is consistent with the alignment of the Fermi levels of the two independent components, but it is not confirmed by the Bader charge analysis, which suggests transfer of >0.01 electrons from the perovskite to the C60. On the other hand, the DOS of both the C60 and $MAPbI_3$ are altered by the perovskite−C60 interaction, with a consistent electronic reorganization when the two materials are in close contact (see Figure 7b). We definitely confirm the hybridization of the $MAPbI_3$ and C60 states by visual inspection of the LUMO orbitals of the C60, which demonstrates a strong hybridization of the two components (see the Supporting Information).

Table 3 summarizes the shift in the vacuum and in the Fermi level and the Bader charge analysis for the $MAPbI_3$ and C60 components. For nearly all the MAI-terminated models, we observe the rise by a few hundredths of an electronvolt in the vacuum level, together with the downshift of the Fermi level going from the isolated $MAPbI_3$ to the interacting $MAPbI_3$/C60 and a charge transfer of 0.01−0.03 electrons from $MAPbI_3$ to C60. All of these results are consistent with a charge transfer from the perovskite to C60. Only for two cases, the apolar−aboveC and apolar−aboveI models, we observe a downshift in the vacuum level that is consistent with the polarization mechanism in Figure 6a. We conclude that, for the MAI-terminated surface, the charge transfer and the polarization mechanism compete in shifting the energy levels of the C60, with the former generally dominating and sourcing an upshift of the C60 levels by a few hundredths of an electronvolt. These findings agree quite well with the UPS/IPES measurements by Schulz et al.,[17] who found an upshift of 0.3 eV of the levels of the C60 when a monolayer is deposited onto the perovskite surface, and a consequent rising of the energy levels of the C60. This results in the reduction of the offset between the CBE of $MAPbI_3$ and the LUMO of C60 from 0.4 to 0.1 eV, which could have both positive and negative effects on the photovoltaic working mechanism. On the one hand, the reduction of the energy level offset is expected to reduce the loss in the open-circuit voltage and to ease the charge injection of the photogenerated charges from the latter to the former, as the states are in closer resonance. On the other hand, the small offset between the LUMO of C60 and the CBE of $MAPbI_3$ also eases the back-transfer of electrons from C60 to $MAPbI_3$ and makes the charge recombination in the perovskite more likely.

For the PbI-terminated surface, we observed hybridization between the states of $MAPbI_3$ and C60 for several slab models (see the Supporting Information). This hybridization results in a downshift of the levels of the C60 for almost all investigated cases with energy variations comprised between 0.05 and 0.43 eV. The results of our simulations on PbI-terminated surfaces nicely parallel the UPS measurements by Lo et al.,[21] who reported unusual energetics for the VBE and CBE of $MAPbI_3$ respectively at 6.4 and 4.7 eV; that is 1 eV below the energies most widely reported in the literature.[16,17,69] On this basis, they proposed the $MAPbI_3$/C60 to be a type I heterojunction, with the band gap of the perovskite embedded by that of the C60, which is exactly the situation depicted in Figure 6d, and we hence suggest that these works probed the PbI-terminated surface. These authors also found a downshift of the C60 levels by 0.16 eV, when the C60 monolayer is deposited onto

DOI: 10.1021/acs.chemmater.6b03259
Chem. Mater. 2017, 29, 958−968

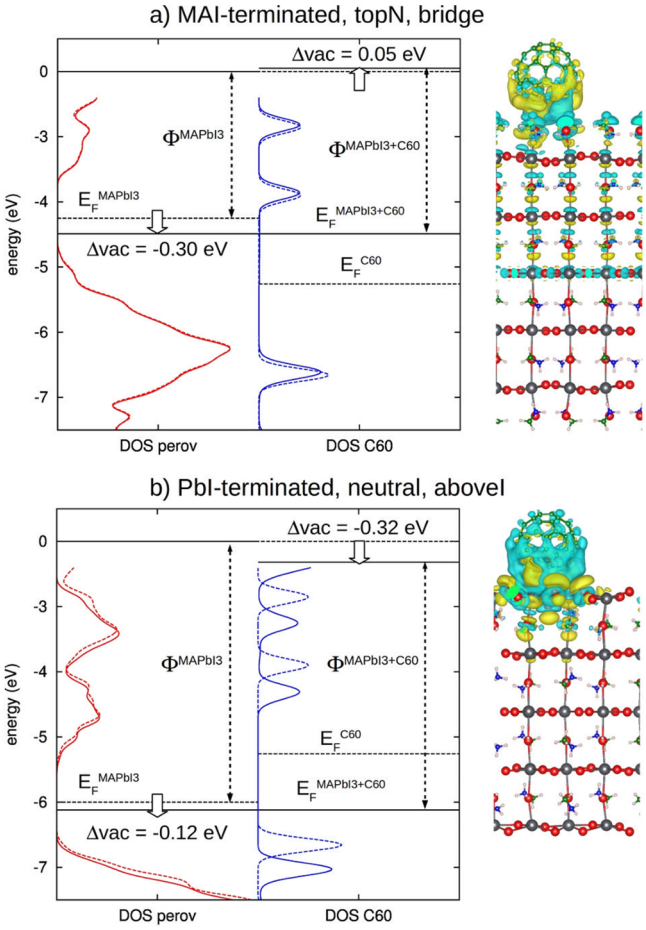

Figure 7. Variation of the DOS and electronic levels (left panels) and of the electronic density (right panel) of two $MAPbI_3$/C60 study cases, going from the noninteracting (dashed line) to the interacting case (solid line): (a) MAI termination, with topN orientation and bridge position for C60; (b) PbI termination, with apolar orientation and aboveI position for C60. The energy levels of both the noninteracting and the interacting systems have been corrected as explained in the main text. For the difference of the electron densities, blue and yellow correspond to depleted and enriched electrons regions, respectively.

$MAPbI_3$, again fully consistent with the downshifts of the vacuum level reported in Table 3 for the PbI-terminated models. This downshift reduces the offset between the LUMO of C60 and CBE of the $MAPbI_3$, but (according to our calculations) it is not sufficient to make the LUMO of the C60 more stable than the CBE of $MAPbI_3$; thus the electron injection from the perovskite to C60 remains unfavorable.

CONCLUSIONS

Surface properties affect the electronic processes going on at the interfaces with semiconductors in most optoelectronic devices. Namely, the energies of the valence and conduction band edges and their matching with hole/electron transporting materials need to be tuned in order to guarantee efficient charge injection/extraction. For the case of the $CH_3NH_3PbI_3$ ($MAPbI_3$) perovskite, which represents one of the most promising materials recently proposed for photovoltaic applications, a detailed rationale of the surface electronic properties is still largely missing. Here, we reported on a DFT study of the energetics and electronic properties of $MAPbI_3$ surfaces, aimed at clarifying the dependence of the VBE and CBE energies on detailed structural parameters, as the orientation of the methylammonium (MA) cations and the termination of the surface, exposing lead and iodide atoms (PbI-terminated) or iodide atoms and MA cations (MAI-terminated). We found that the surface termination profoundly impacts the energy of the frontier electronic levels, with PbI-terminated models showing valence and conduction band edges ~1 eV lower in energy that the corresponding states in MAI-terminated models most widely probed experimentally.[29,30] Note that such changes in the energy position of the frontier crystal orbitals are defined with respect to the vacuum level.

The existence of two surfaces with very different energy positioning of their frontier electronic levels has dramatic impact on the energy level alignment of $MAPbI_3$ with respect to the electrodes and the hole and electron transport materials. To illustrate this concept, we performed DFT simulations on the interface between MAPbI3 and C60, which, thanks to its positive photovoltaic performances[31] and negligible hysteretic behavior,[32] represents a highly relevant case study. For noninteracting $MAPbI_3$/C60, the CBE of the MAI-terminated perovskite lies above the LUMO of the C60, allowing for a spontaneous charge transfer of the photogenerated electron into the C60, while the CBE of the PbI-terminated perovskite lies below the LUMO of the C60, instead hindering electron injection. When the C60 interacts with the MAI-terminated surface, it shows an upshift of its electronic levels, due to a charge transfer from the perovskite to the C60, which reduces

Table 3. Shift of the Vacuum Level (Δvac) and Charge Transfer on $MAPbI_3$ and C60, upon Going from the Non-interacting to the Interacting Case[a]

model			charge[b]	
$MAPbI_3$	C60	Δvac (eV)	$MAPbI_3$	C60
		MAI-Terminated		
apolar	aboveC	−0.08	−0.01	0.01
	aboveI	−0.07	0.02	−0.02
	aboveN	−0.02	0.00	0.00
	bridge	0.03	0.03	−0.02
topC	aboveC	0.00	0.00	0.00
	aboveI	0.01	0.01	−0.01
	bridge	0.03	0.03	−0.02
topN	aboveC	0.00	0.00	0.00
	aboveI	0.02	0.02	−0.01
	bridge	0.05	0.02	−0.02
		PbI-Terminated		
apolar	aboveC	−0.07	0.04	−0.04
	aboveI	−0.32	0.01	−0.06
	aboveN	0.02	0.04	−0.03
	abovePb	−0.16	−0.01	0.02
topC	aboveC	−0.43	0.03	−0.02
	aboveI	−0.29	−0.01	0.02
	abovePb	−0.24	−0.03	0.04
topN	aboveI	−0.05	−0.01	0.01
	aboveN	−0.13	0.02	−0.02
	abovePb	−0.16	0.00	0.00

[a]The charge is the difference in the nominal number of electrons and that obtained from the Bader analysis, and it is positive for electron lacking systems. [b]For some cases, the charge on the two components is not exactly the opposite, because the Bader charge does not normalize to the nominal charge (error of ~0.01 electrons over thousands).

DOI: 10.1021/acs.chemmater.6b03259
Chem. Mater. 2017, 29, 958−968

the offset between the perovskite CBE and the C60 LUMO but does not invert their ordering in energy, thus preserving the condition for spontaneous electron injection. This upshift and the consequent reduction of the energy level offset nicely parallels the measurements from Schulz et al.[17] and is expected, on the one hand, to ease the injection of the photogenerated charges from the perovskite to the C60 but, on the other hand, also to ease back-transfer from the C60 back to the perovskite, thus facilitating the charge recombination at the interface. When the C60 interacts with the PbI-terminated surface, instead, it shows a downshift of its electronic levels, mostly because of the mixing/hybridization between the C60 and the perovskite states. This downshift is consistent with experimental data from Lo et al.[21] and brings the LUMO level of the C60 closer to the CBE of the perovskite (yet, from our calculations, this is not enough to exchange their relative energies, thus leaving the electron injection from the perovskite to the C60 an endothermic process in this case). It is worth mentioning that a very recent work by Jacobs et al. also pointed out the importance of the surface termination in the determination of the energy of the electronic levels for perovskite oxides.[70]

The results of the present work bear important implications for the design of efficient perovskite-based photovoltaic devices, as they point to the importance of a fine control of the surface termination. Here, we showed that $MAPbI_3$ exposing MAI-rich layers is more thermodynamically stable than PbI-terminated surfaces and features a more favorable energy level alignment for electron extraction using fullerene electron transporting materials. It has been, however, demonstrated that moisture induces surface degradations prompting the removal of the upper organic-rich layers and the formation of unfavorable (for electron extraction purposes) PbI-terminated surfaces.[25]

■ ASSOCIATED CONTENT

Supporting Information

The Supporting Information is available free of charge on the ACS Publications website at DOI: 10.1021/acs.chemmater.6b03259.

Starting orientation of the MA cations in the MAI-terminated and topN model and after relaxation with vdw-DF2 and PBE, procedure for the calculation of the relative stability of the $MAPbI_3$ slab models, energy of the valence and conduction band edge in (110) surfaces and for thin, $3PbI_2$- and $7PbI_2$-layered models, and C60 LUMO orbitals for three selected PbI-terminated slab models (PDF)

■ AUTHOR INFORMATION

Corresponding Author

*E-mail: claudio.quarti@umons.ac.be.

ORCID

Claudio Quarti: 0000-0002-5488-1216

Notes

The authors declare no competing financial interest.

■ ACKNOWLEDGMENTS

The work was supported by the Interuniversity Attraction Pole program of the Belgian Federal Science Policy Office (PAI 6/27) and FNRS-F.R.S. Computational resources have been provided by the Consortium des Équipements de Calcul Intensif (CÉCI), funded by the Fonds de la Recherche Scientifique de Belgique (F.R.S.-FNRS) under Grant No. 2.5020.11. D.B. is a FNRS Research Director.

■ REFERENCES

(1) Kojima, A.; Teshima, K.; Shirai, Y.; Miyasaka, T. Organometal Halide Perovskites as Visible-Light Sensitizers for Photovoltaic Cells. *J. Am. Chem. Soc.* **2009**, *131*, 6050−6051.

(2) Im, J.-H.; Lee, C.-R.; Lee, J.-W.; Park, S.-W.; Park, N.-G. 6.5% Efficient Perovskite Quantum-Dot-Sensitized Solar Cell. *Nanoscale* **2011**, *3*, 4088−4093.

(3) Burschka, J.; Pellet, N.; Moon, S.-J.; Humphry-Baker, R.; Gao, P.; Nazeeruddin, M. K.; Graetzel, M. Sequential Deposition as a Route to High-Performance Perovskite-Sensitized Solar Cells. *Nature* **2013**, *499*, 316−319.

(4) Liu, M.; Johnston, M. B.; Snaith, H. J. Efficient Planar Heterojunction Perovskite Solar Cells by Vapour Deposition. *Nature* **2013**, *501*, 395−398.

(5) Zhou, H.; Chen, Q.; Li, G.; Luo, S.; Song, T.-B.; Duan, H.-S.; Hong, Z.; You, J.; Liu, Y.; Yang, Y. Interface engineering of highly efficient perovskite solar cells. *Science* **2014**, *345*, 542−546.

(6) Jeon, N. J.; Noh, J. H.; Yang, W. S.; Kim, Y. C.; Ryu, S.; Seo, J.; Seok, S. I. Compositional engineering of perovskite materials for high-performance solar cells. *Nature* **2015**, *517*, 476−480.

(7) Noh, J. H.; Im, S.-H.; Heo, H. H.; Mandal, T. N.; Seok, S. I. Chemical management for colorful, efficient, and stable inorganic-organic hybrid nanostructured solar cells. *Nano Lett.* **2013**, *13*, 1764−1769.

(8) Stranks, S. D.; Eperon, G. E.; Grancini, G.; Menelaou, C.; Alcocer, M. J. P.; Leijtens, T.; Herz, L. M.; Petrozza, A.; Snaith, H. J. Electron-Hole Diffusion Lengths Exceeding 1 Micrometer in an Organometal Trihalide Perovskite Absorber. *Science* **2013**, *342*, 341−344.

(9) Edri, E.; Kirmayer, S.; Henning, A.; Mukhopadhyay, S.; Gartsman, K.; Rosenwaks, Y.; Hodes, G.; Cahen, D. Why lead methylammonium tri-iodide perovskite-based colar cells require a mesoporous electron transporting scaffold (but not necessarily a hole conductor). *Nano Lett.* **2014**, *14*, 1000−1004.

(10) Edri, E.; Kirmayer, S.; Mukhopadhyay, S.; Gartsman, K.; Hodes, G.; Cahen, D. Elucidating the charge carrier separation and working mechanism of $CH_3NH_3PbI_{3-x}Cl_x$ perovskite solar cells. *Nat. Commun.* **2014**, *5*, 3461.

(11) Karakus, M.; Jensen, S. A.; D'Angelo, F.; Turchinovich, D.; Bonn, M.; Canovas, E. Phonon-electron scattering limits free charge mobility in methylammonium lead iodide perovskites. *J. Phys. Chem. Lett.* **2015**, *6*, 4991−4996.

(12) Ponseca, C. S.; Savenije, T. J.; Abdellah, M.; Zheng, K.; Yartsev, A.; Pascher, T.; Harlang, T.; Chabera, T.; Pullerits, T.; Stepanov, A.; Wolf, J.-P.; Sundström, V. Organometal Halide Perovskite Solar Cell Materials Rationalized: Ultrafast Charge Generation, High and Microsecond-Long Balanced Mobilities, and Slow Recombination. *J. Am. Chem. Soc.* **2014**, *136*, 5189−5192.

(13) Savenije, T. J.; Ponseca, C. S., Jr.; Kunneman, L.; Abdellah, M.; Zheng, K.; Tian, Y.; Zhu, Q.; Canton, S. E.; Scheblykin, I. G.; Pullerits, T.; Yartsev, A.; Sundström, V. Thermally Activated Exciton Dissociation and Recombination Control the Carrier Dynamics in Organometal Halide Perovskite. *J. Phys. Chem. Lett.* **2014**, *5*, 2189−2194.

(14) De Wolf, S.; Holovsky, J.; Moon, S.-J.; Löper, P.; Niesen, B.; Ledinsky, M.; Haug, F.-J.; Yum, J.-H.; Ballif, C. Organometallic halide perovskites: Sharp optical absorption edge and its relation to photovoltaic performance. *J. Phys. Chem. Lett.* **2014**, *5*, 1035−1039.

(15) Wehrenfennig, C.; Eperon, G. E.; Johnston, M. B.; Snaith, H. J.; Herz, L. M. High Charge Carrier Mobilities and Lifetimes in Organolead Trihalide Perovskites. *Adv. Mater.* **2014**, *26*, 1584−1589.

(16) Schulz, P.; Edri, E.; Kirmayer, S.; Hodes, G.; Cahen, D.; Kahn, A. Interface energetics in organo-metal halide perovsite-based photovoltaic cells. *Energy Environ. Sci.* **2014**, *7*, 1377−1381.

DOI: 10.1021/acs.chemmater.6b03259
Chem. Mater. 2017, 29, 958−968

(17) Schulz, P.; Whittaker-Brooks, L. L.; MacLeod, B. A.; Olson, D. C.; Loo, Y.-L.; Kahn, A. Electronic level alignment in inverted organometal perovskite solar cells. *Adv. Mater. Interfaces* **2015**, *2*, 1400532.
(18) Schulz, P.; Dowgiallo, A.-M.; Yang, M.; Zhu, K.; Blackburn, J. L.; Berry, J. J. Charge transfer dynamics between carbon nanotubes and hybrid organic metal halide perovskite films. *J. Phys. Chem. Lett.* **2016**, *7*, 418−425.
(19) Yin, J.; Cortecchia, D.; Krishna, A.; Chen, S.; Mathews, N.; Grimsdale, A. G.; Soci, C. Interfacial charge transfer anisotropy in polycrystalline lead iodide perovskite films. *J. Phys. Chem. Lett.* **2015**, *6*, 1396−1402.
(20) Liu, X.; Wang, C.; Lyu, L.; Wang, C.; Xiao, Z.; Bi, C.; Huang, J.; Gao, Y. Electronic structures at the interface between Au and $CH_3NH_3PbI_3$. *Phys. Chem. Chem. Phys.* **2015**, *17*, 896−902.
(21) Lo, M.-F.; Guan, Z.-Q.; Ng, T.-W.; Chan, C.-Y.; Lee, C.-S. Electronic structures and photoconversion mechanism in perovskite/fullerene heterojunctions. *Adv. Funct. Mater.* **2015**, *25*, 1213−1218.
(22) Miller, E. M.; Zhao, Y.; Mercado, C. C.; Saha, S. K.; Luther, J. M.; Zhu, K.; Stevanovic, V.; Perkins, C. L.; van de Lagemaat, J. Substrate-controlled band positions in $CH_3NH_3PbI_3$ perovskite films. *Phys. Chem. Chem. Phys.* **2014**, *16*, 22122−22130.
(23) Haruyama, J.; Sodeyama, K.; Han, L.; Tateyama, Y. Termination dependence of tetragonal $CH_3NH_3PbI_3$ surface for perovskite solar cells. *J. Phys. Chem. Lett.* **2014**, *5*, 2903−2909.
(24) Yang, J.; Siempelkamp, B. D.; Liu, D.; Kelly, T. L. Investigation of $CH_3NH_3PbI_3$ degradation rages and mechanisms in controlled humidity environments using in situ techniques. *ACS Nano* **2015**, *9*, 1955−1963.
(25) Mosconi, E.; Azpiroz, J. M.; De Angelis, F. Ab initio molecular dynamics simulations of methylammonium lead iodide perovskite degradation by water. *Chem. Mater.* **2015**, *27*, 4885−4892.
(26) Koocher, N. Z.; Saldana-Greco, D.; Wang, F.; Liu, S.; Rappe, A. M. Polarization dependence of water adsorption to $CH_3NH_3PbI_3$ (001) surfaces. *J. Phys. Chem. Lett.* **2015**, *6*, 4371−4378.
(27) Bryant, D.; Aristidou, N.; Pont, S.; Sanchez-Molina, I.; Chotchunangatchaval, T.; Wheeler, S.; Durrant, J. R.; Haque, S. A. Light and oxygen induced degradation limits the operational stability of methylammonium lead triiodide perovskite solar cells. *Energy Environ. Sci.* **2016**, *9*, 1655−1660.
(28) Foley, B. J.; Marlowe, K. S.; Sun, K.; Saidi, W. A.; Scudiero, L.; Gupta, m. c.; Choi, J. J. Temperature dependent energy levels of methylammonium lead iodide perovskite. *Appl. Phys. Lett.* **2015**, *106*, 243904.
(29) She, L.; Liu, M.; Zhong, D. Atomic structures of $CH_3NH_3PbI_3$ (001) surfaces. *ACS Nano* **2016**, *10*, 1126−1131.
(30) Ohmann, R.; Ono, L. K.; Kim, H.-S.; Lin, H.; Lee, M. V.; Li, Y.; Park, N.-G.; Qi, Y. Real-space imaging of the atomic structure of organic-inorganic perovskite. *J. Am. Chem. Soc.* **2015**, *137*, 16049−16054.
(31) Liang, P.-W.; Chueh, C.-C.; Williams, S. T.; Jen, A. K.-Y. Roles of fullerene-based interlayers in enhancing the performance of organometal perovskite thin-film solar cells. *Adv. Energy Mater.* **2015**, *5*, 1402321.
(32) Xu, J.; Buin, A.; Ip, A. H.; Li, W.; Voznyy, A.; Comin, R.; Yuan, M.; Jeon, S.; Ning, Z.; McDowell, J. J.; Kanjanaboos, P.; Sun, J.-P.; Lan, X.; Quan, L. N.; Kim, D. H.; Hill, I. G.; Maksymovych, P.; Sargent, E. Perovskite-fullerene hybrid materials suppress hysteresis in planar diodes. *Nat. Commun.* **2015**, *6*, 7081.
(33) Poglitsch, A.; Weber, D. Dynamic Disorder in Methylammoniumtrihalogenoplumbates (II) Observed by Millimeterwave Spectroscopy. *J. Chem. Phys.* **1987**, *87*, 6373−6378.
(34) Quarti, C.; Mosconi, E.; De Angelis, F. Interplay of Orientational Order and Electronic Structure in Methylammonium Lead Iodide: Implications for Solar Cells Operation. *Chem. Mater.* **2014**, *26*, 6557−6569.
(35) Motta, C.; El-Mellouhi, F.; Kais, S.; Tabet, N.; Alharbi, F.; Sanvito, S. Revealing the role of organic cations in hybrid halide perovskite $CH_3NH_3PbI_3$. *Nat. Commun.* **2015**, *6*, 7026.
(36) Amat, A.; Mosconi, E.; Ronca, E.; Quarti, C.; Umari, P.; Nazeeruddin, M. K.; Graetzel, M.; De Angelis, F. Cation-Induced band gap tuning in organohalide perovskites: interplay of spin-orbit coupling and octahedral tilting. *Nano Lett.* **2014**, *14*, 3608−3616.
(37) Stroppa, A.; Quarti, C.; De Angelis, F.; Picozzi, S. Ferroelectric polarization of $CH_3NH_3PbI_3$: a detailed study based on density functional theory and symmetry mode analysis. *J. Phys. Chem. Lett.* **2015**, *6*, 2223−2231.
(38) Zheng, F.; Takenaka, H.; Wang, F.; Koocher, N. Z.; Rappe, A. M. First-principles calcualtion of the bulk photovoltaic effect in $CH_3NH_3PbI_3$ and $CH_3NH_3PbI_{3-x}Cl_x$. *J. Phys. Chem. Lett.* **2015**, *6*, 31−37.
(39) Frost, J. M.; Butler, K. T.; Walsh, A. Molecular ferroelectric contributions to anomalous hysteresis in hybrid perovskite solar cells. *APL Mater.* **2014**, *2*, 081506.
(40) Brivio, F.; Butler, K. T.; Walsh, A.; van Schilfgaarde, M. Relativistic Quasiparticle Self-Consistent Electronic Structure of Hybrid Halide Perovskite Photovoltaic Absorbers. *Phys. Rev. B: Condens. Matter Mater. Phys.* **2014**, *89*, 155204−6.
(41) Stroppa, A.; Di Sante, D.; Barone, P.; Bokdam, M.; Kresse, G.; Franchini, C.; Whangbo, M.-H.; Picozzi, S. Tunable ferroelectric polarization and its interplay with spin-orbit coupling in tin iodide perovskites. *Nat. Commun.* **2014**, *5*, 5900.
(42) Kutes, J.; Ye, L.; Zhou, Y.; Pang, S.; Huey, B. E.; Padture, N. P. Direct observation of ferroelectric domains in solution-processed $CH_3NH_3PbI_3$ perovskite thin films. *J. Phys. Chem. Lett.* **2014**, *5*, 3335−3339.
(43) Wasylishen, R. E.; Knop, O.; Macdonald, J. B. Cation rotation in methylammonium lead halides. *Solid State Commun.* **1985**, *56*, 581−582.
(44) Mattoni, A.; Filippetti, A.; Saba, M. I.; Delugas, P. Methylammonium rotational dynamics in lead halide perovskite by classical molecular dynamics: the role of temperature. *J. Phys. Chem. C* **2015**, *119*, 17421−17428.
(45) Persson, P.; Gebhardt, J. C. M.; Lunell, S. The Smallest Possible Nanocrystals of Semiionic Oxides. *J. Phys. Chem. B* **2003**, *107*, 3336−3339.
(46) Lundqvist, M. J.; Nilsing, M.; Persson, P.; Lunell, S. DFT study of bare and dye-sensitized TiO2 clusters and nanocrystals. *Int. J. Quantum Chem.* **2006**, *106*, 3214−3234.
(47) De Angelis, F.; Di Valentin, C.; Fantacci, S.; Vittadini, A.; Selloni, A. Theoretical Studies on Anatase and Less Common TiO_2 Phases: Bulk, Surfaces, and Nanomaterials. *Chem. Rev.* **2014**, *114*, 9708−9753.
(48) Giannozzi, P.; et al. QUANTUM ESPRESSO: a Modular and Open-Source Software Project for Quantum Simulations of Materials. *J. Phys.: Condens. Matter* **2009**, *21*, 395502.
(49) Lee, K.; Murray, E. D.; Kong, L.; Lundqvist, B. I.; Langreth, D. C. Higher-accuracy van der Waals density functional. *Phys. Rev. B: Condens. Matter Mater. Phys.* **2010**, *82*, 081101.
(50) Vanderbilt, D. Soft Self-Consistent Pseudopotentials in a Generalized Eigenvalue Formalism. *Phys. Rev. B: Condens. Matter Mater. Phys.* **1990**, *41*, 7892−7895.
(51) Quarti, C.; Mosconi, E.; De Angelis, F. Structural and electronic properties of organo-halide hybrid perovskites from ab initio molecular dynamics. *Phys. Chem. Chem. Phys.* **2015**, *17*, 9394−9409.
(52) Tang, W.; Sanville, E.; Henkelman, G. A grid-based Bader analysis algorithm without lattice bias. *J. Phys.: Condens. Matter* **2009**, *21*, 084204.
(53) Bengtsson, L. Dipole correction for surface supercell calculations. *Phys. Rev. B: Condens. Matter Mater. Phys.* **1999**, *59*, 12301.
(54) Grimme, S. Semiempirical GGA-type density functional constructed with a long-range dispersion correction. *J. Comput. Chem.* **2006**, *27*, 1787−1799.
(55) D'Innocenzo, V.; Grancini, G.; Alcocer, M. J. P.; Kandada, A. R. S.; Stranks, S. D.; Lee, M. M.; Lanzani, G.; Snaith, H. J.; Petrozza, A. Excitons versus free charges in organo-lead tri-halide perovskites. *Nat. Commun.* **2014**, *5*, 3586.

DOI: 10.1021/acs.chemmater.6b03259
Chem. Mater. 2017, 29, 958−968

(56) Umebayashi, T.; Asai, K.; Kondo, T.; Nakao, A. Electronic structures of lead iodide based low-dimensional crystals. *Phys. Rev. B: Condens. Matter Mater. Phys.* **2003**, *67*, 155405.
(57) Mosconi, E.; Amat, A.; Nazeeruddin, M. K.; Graetzel, M.; De Angelis, F. First-Principles Modeling of Mixed Halide Organometal Perovskites for Photovoltaic Applications. *J. Phys. Chem. C* **2013**, *117*, 13902−13913.
(58) Even, J.; Pedesseau, L.; Jancu, J.-M.; Katan, C. Importance of Spin−Orbit Coupling in Hybrid Organic/Inorganic Perovskites for Photovoltaic Applications. *J. Phys. Chem. Lett.* **2013**, *4*, 2999−3005.
(59) Menéndez-Proupin, E.; Palacios, P.; Wahnon, P.; Conesa, J. C. Self-consistent relativistic band structure of the $CH_3NH_3PbI_3$ perovskite. *Phys. Rev. B: Condens. Matter Mater. Phys.* **2014**, *90*, 045207.
(60) Umari, P.; Mosconi, E.; De Angelis, F. Relativistic GW Calculations on $CH_3NH_3PbI_3$ and $CH_3NH_3SnI_3$ Perovskites for Solar Cell Applications. *Sci. Rep.* **2014**, *4*, 4467.
(61) Heimel, G.; Salzmann, I.; Duhm, S.; Koch, N. Design of organic semiconductors from molecular electrostatics. *Chem. Mater.* **2011**, *23*, 359−377.
(62) Junquera, J.; Zimmer, M.; Ordéjon, P.; Ghosez, P. First-principle calculation of the band offset at $BaO/BaTiO_3$ and $Sr/SrTiO_3$ interfaces. *Phys. Rev. B: Condens. Matter Mater. Phys.* **2003**, *67*, 155327.
(63) Toroker, M. C.; Kanan, D. K.; Alidoust, N.; Isseroff, L. Y.; Liao, P.; Carter, E. A. First principle scheme to evaluate band edge positions in potential transition metal oxide photocatalysts and photoelectrodes. *Phys. Chem. Chem. Phys.* **2011**, *13*, 16644−16654.
(64) Singh-Miller, N. E.; Marzari, N. Surface energies, work functions and surface relaxations of low-index metallic surfaces from first principles. *Phys. Rev. B: Condens. Matter Mater. Phys.* **2009**, *80*, 235407.
(65) Cahen, D.; Kahn, A. Electron energetics at surfaces and interfaces: concepts and experiments. *Adv. Mater.* **2003**, *15*, 271−277.
(66) Galimberti, D.; Quarti, C.; Milani, A. Polymorphism of even nylons revisited through periodic quantum chemical calculations. *Polymer* **2015**, *67*, 167−173.
(67) Shirley, E. L.; Louie, S. Electron excitations in solid C60: energy gap, band dispersions, and effects of orientational disorder. *Phys. Rev. Lett.* **1993**, *71*, 133.
(68) Qian, X.; Umari, P.; Marzari, N. First-principles investigation of organic photovoltaic materials C_{60}, C_{70}, $[C_{60}]$PCBM, and bis-$[C_{60}]$PCBM using a many-body G_0W_0-Lanczos approach. *Phys. Rev. B: Condens. Matter Mater. Phys.* **2015**, *91*, 245105.
(69) Qin, P.; Paek, S.; Dar, M. I.; Pellet, N.; Ko, J.; Graetzel, M.; Nazeeruddin, M. K. Perovskite solar cells with 12.8% efficiency by using conjugated quinolizino acridine based hole transporting materials. *J. Am. Chem. Soc.* **2014**, *136*, 8516−8519.
(70) Jacobs, R.; Booske, J.; Morgan, D. Understanding and controlling the work function of perovskite oxides using density functional theory. *Adv. Funct. Mater.* **2016**, *26*, 5471−5482.

DOI: 10.1021/acs.chemmater.6b03259
Chem. Mater. 2017, 29, 958−968